

Tsunami Propagation from a Finite Source

George F. Carrier¹ and Harry Yeh²

Abstract: Sea-bottom displacements associated with seismic events are confined largely to strips of large but finite aspect ratio. We analyze waves that are initiated on such a strip and that propagate across a region of finite depth. We invoke the classical shallow-water-wave theory to obtain rather comprehensive descriptions of the non-dispersive aspects of the waves. The directivity of the energy radiation and the domain of pulse persistence are discussed.

keyword: Tsunami, Directivity

1 Introduction

Sea-floor displacements associated with subduction-type seismic ruptures are often elongated in the strike direction – the direction in which the fault plane intersects the horizontal plane. Under such a circumstance, directivity of tsunami propagation is well recognized; the azimuthal dependence of the energy radiation is affected by the orientation of a tsunami source of a finite length; tsunami energy tends to radiate in the direction perpendicular to the major axis of the elongated source. This characteristic was experimentally examined by Takahashi and Hatori (1962) who observed wave propagation from an elliptic-shape source. Many case studies by numerical simulations clearly exhibit the directivity (e.g. the 1960 Chilean Tsunami, the 1964 Alaskan Tsunami, and the 2004 Sumatran Tsunami). It appears the more elongated the source is, the stronger the directivity. Based on the work by Ben-Menahem (1961) on the azimuthal dependence of seismic-wave radiation, Okal (2003) demonstrated that a tsunami generated by instantaneous sea-floor displacement has a strong directivity pattern in the direction normal to the seismic dislocation. Using a Green's function technique, Kajiura (1970) solved this problem for tsunamis generated by uniform or linear bottom deformation of a rectangular shape with a constant vertical velocity of the bottom movement. In spite of his

formal treatment, Kajiura's method is difficult to obtain a quantitative solution accurately for the displacement with a large ratio of the side lengths of the rectangle: for this reason, he only computed the cases with the aspect ratio up to 3. We take a different approach from Kajiura (1970) to obtain a quantitative description of the tsunami propagation, including the cases with the very large aspect ratio. A convenient self-similar expression is derived from the exact solution of the axisymmetrical problem, thereby the complete propagation field generated from a finite source can be efficiently computed.

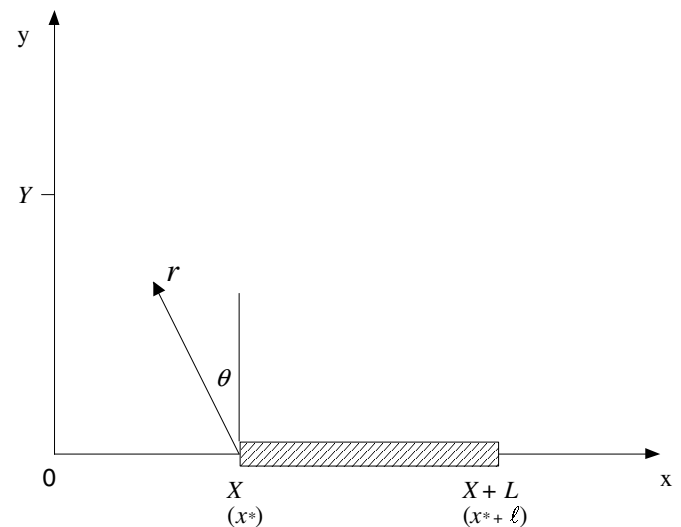


Figure 1 : A definition sketch for wave-field configuration indicating the dimensional coordinates (x^* , $x^* + l$) of source domain, and dimensionless source location ($X, X + L$). A wave arrival locale of interest is indicated by $Y = y(x = 0)$.

A schematic plan-view sketch of the initial tsunami source configuration is depicted in Fig. 1. The occurrence of a sudden, seismically generated, vertical excursion of a segment (x^* , $x^* + l$) of the sea floor implies an almost simultaneous vertical displacement of the sea surface and the gravity wave so initiated radiates outward from that source. When the displaced segment of the

¹ deceased

² Oregon State University, Corvallis, OR 97331, USA

seafloor lies in deep water but has lateral dimensions that are large compared to the depth, and the displacement time scale is much shorter than (or negligible to) the flow-establishment time scale, the initial surface displacement has a static deformation with a shape that is a smoothed replica of the sea-floor displacement. More precisely, the ratio of the magnitude of the spectral intensity of the surface displacement to that of the sea-floor displacement is of the order $\cosh^{-1}(kh)$, where k is the wave number and h is the depth of the water; we consider $kh \rightarrow 0$. The propagating wave undergoes a dispersion in which, when the wave has traveled a distance q from its source, the spectral contributions whose wavelengths are small compared to $(q/h)^{1/3}h$ have traveled so slowly that they no longer contribute to the shape or intensity of the energetic leading wave system away from the tsunami source (Carrier, 1966, 1971). For a very large tsunami generated by a giant earthquake ($M_w > 8.5$, e.g. the 1960 Chile Earthquake, the 1964 Great Alaska Earthquake, and the 2004 Sumatran Earthquake), the breadth of the sea floor displacement is sufficiently large – the leading wavelength is very long $O(100 \text{ km})$ – and the vertical displacement is small, less than several meters.

Hence, both frequency and amplitude dispersion have negligible effects on the leading wave as it propagates across an ocean. For example, suppose a tsunami 150 km long and 2.0 m high occurs in an ocean 3,500 m deep, then, based on the criteria proposed by Hammack and Segur (1978), the interval of applicability of linear non-dispersive long-wave theory is approximately 13,000 km, which is about the diameter of the Earth (\approx the longest distance across the Pacific Ocean). Note that the tsunami wavelength recorded for the 2004 Sumatran tsunami was approximately 450 km! Such a very long wave can propagate in a distance equal to three times the Earth's circumference without frequency-dispersion effect. Hence, the use of linear non-dispersive long-wave theory is justified to study tsunami propagation in deep oceans.

Seismic fault rupture is not instantaneous in reality, but the speed is finite; the finite speed of the sea floor displacement influences the directivity of tsunami propagation. This characteristic can be explained by the analogy to the shock-front formation generated by a fast moving disturbance in shallow water. However, the fault rupture speed ($V \sim 2.5 \text{ km/sec}$) is much faster than the speed of water-wave propagation ($c \sim 0.2 \text{ km/sec}$ in abyssal plain). The offset angle deviated from the case of in-

stantaneous rupture is very small, i.e., $\sin^{-1}c/V \sim 5^\circ$, which is considered negligibly small. Accordingly, nothing of importance is lost when we postulate for our analysis a family of instantaneous water-surface displacements whose spectra are already devoid of short wavelength contributions.

2 Analysis

Classical linear long-wave theory suggests that the water-surface displacement η of waves whose lateral characterizing dimensions are large compared to the depth can be approximated by solutions of

$$gh \Delta^* \eta^* - \eta_{r^* t^*}^* = 0, \quad (1)$$

where Δ^* is the Laplace operator in dimensional coordinates, h is the depth, t^* is the time, g is the gravitational acceleration, and the letter subscript denotes partial differentiation. Our primary interest is focused on seafloor displacements that are confined to a strip of length l aligned in x as shown in the definition sketch, Fig. 1.

2.1 Axisymmetric Waves

Prior to considering an initial condition of an elongated source, we first analyze the axisymmetric problem. It is advantageous to scale $x = x^*/\beta$, $y = y^*/\beta$, $r^2 = x^2 + y^2$, $t = \sqrt{gh}t^*/\beta$, and $\eta = \eta^*/\alpha$, where α is the characteristic source amplitude and β is the characteristic source breadth. The axisymmetric solution $\eta(r, t)$ is defined by

$$\frac{1}{r}(r\eta_r)_r - \eta_{tt} = 0 \quad \text{in } t > 0, \quad 0 \leq r < \infty \quad (2)$$

with initial conditions:

$$\eta(r, t = 0) = P(r), \quad \text{and} \quad \eta_t(r, t = 0) = F(r). \quad (3)$$

Note that $F(r) = 0$ for the present problem, but we keep it for generality of the analysis. Following Carrier, Wu, and Yeh (2003), (2) and (3) are solved with the Fourier-Bessel transform, and the inversion gives:

$$\eta(r, t) = \int_0^\infty P(b) \frac{\partial}{\partial t} G(b, r, t) db + \int_0^\infty F(b) G(b, r, t) db, \quad (4)$$

where

$$G(b, r, t) = b \int_0^\infty J_0(\rho r) \sin \rho t J_0(\rho b) d\rho. \quad (5)$$

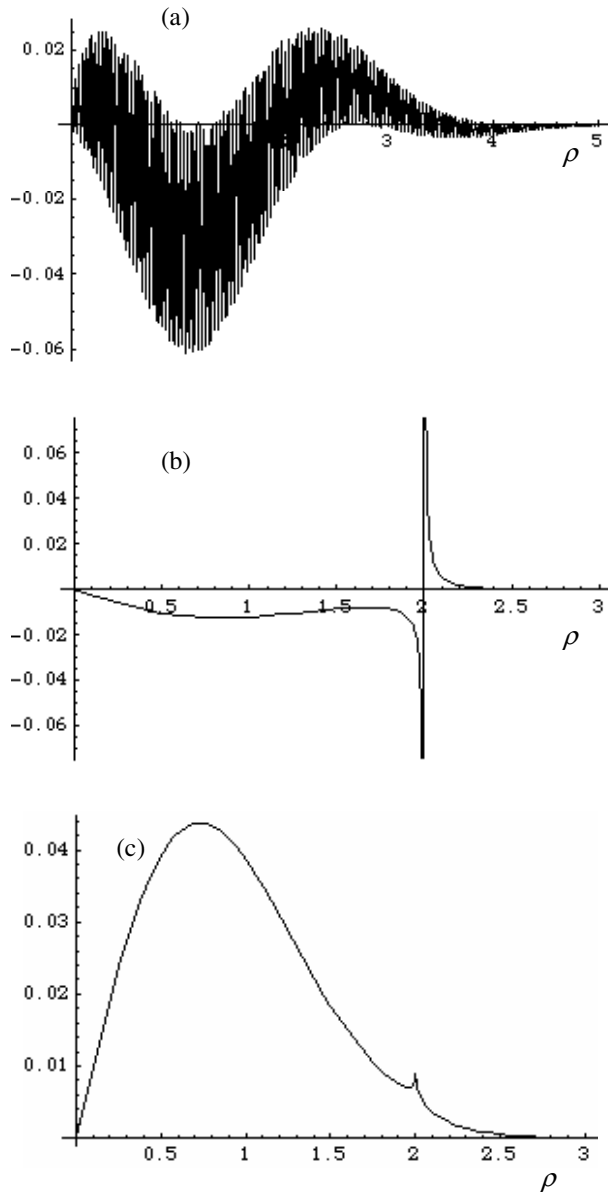


Figure 2 : Plots of the integrand of a) (7), b) (8), and c) (9). $t = 102$, $r = 100$

Equations (4) and (5) yield the general solution to the two-dimensional axisymmetric wave equation.

For this investigation it is convenient to introduce one particular solution and the wave generation for the strip source region will be constructed using this solution, and could be constructed as a superposition of individual displacements each of whose y dependence is e^{-y^2} , namely,

$$\eta(r,0) = P(r) = 2e^{-r^2} \text{ and } \eta_t(r,0) = F(r) = 0. \quad (6)$$

Here we took the amplitude scaling parameter $\alpha = a^*/2$ for convenience, where a^* is the maximum water-surface displacement at $r = 0$. Substituting (6) into (4), the exact integral representation of the solution is found to be:

$$\begin{aligned} \eta(r,t) &= \int_0^\infty \rho J_0(\rho r) \cos \rho t \left(\int_0^\infty 2b J_0(\rho b) e^{-b^2} db \right) d\rho \\ &= \int_0^\infty \rho J_0(\rho r) \cos \rho t e^{-\rho^2/4} d\rho. \end{aligned} \quad (7)$$

While this integral is well behaved for small values of r and t , it becomes formidable to compute for large values of r and t as demonstrated in Fig. 2a. A more convenient form for the integration can be found by the explicit solution to the integral G in (5):

$$\eta(r,t) = \int_0^\infty 2e^{-\rho^2} G_t(\rho, r, t) d\rho \quad (8)$$

$$= \frac{\partial}{\partial t} \int_0^\infty 2e^{-\rho^2} G(\rho, r, t) d\rho, \quad (9)$$

where

$$G(\rho, r, t) = \begin{cases} \frac{2\rho}{\pi\sqrt{t^2-(r-\rho)^2}} K\left(\frac{4r\rho}{t^2-(r-\rho)^2}\right) & \text{for } t > r + \rho \\ \frac{1}{\pi} \sqrt{\frac{\rho}{r}} K\left(\frac{t^2-(r-\rho)^2}{4r\rho}\right) & \text{for } |r-\rho| < t < r + \rho \\ 0 & \text{for } t < |r-\rho| \end{cases} \quad (10)$$

in which $K(k) = \int_0^{\pi/2} \frac{dv}{\sqrt{1-k\sin^2 v}}$ is the Complete Elliptic Integral of the first kind. (Note that (10) was derived previously by Carrier, Wu, and Yeh (2003).) The integrand in (8) is plotted in Fig. 2b, which demonstrates an accurate numerical integration even for large values of r and t ; the singularity that appears in the plot can readily be handled by the standard software packages. Even more accurate numerical integration could be achieved with the use of (9) as seen in the plot of the integrand in Fig. 2c.

Figure 3 shows solutions of (9) for a variety of r and t : Fig. 3a for the early evolution of a Gaussian water-surface displacement (6), and Fig. 3b for its evolution for later time. As expected for the linear non-dispersive wave theory, the radiating waveform appears to become self-similar as early as, say $t > 5$.

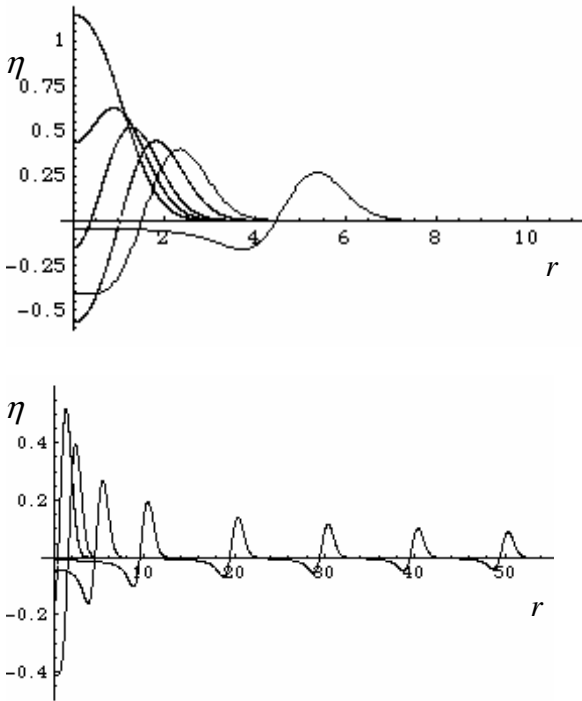


Figure 3 : The evolution of radiating water-surface profiles by solving (9): a) $t = 0.5, 0.75, 1.0, 1.5, 2.0, 5.0$; b) $t = 1.0, 2.0, 5.0, 10.0, 20.0, 30.0, 40.0, 50.0$

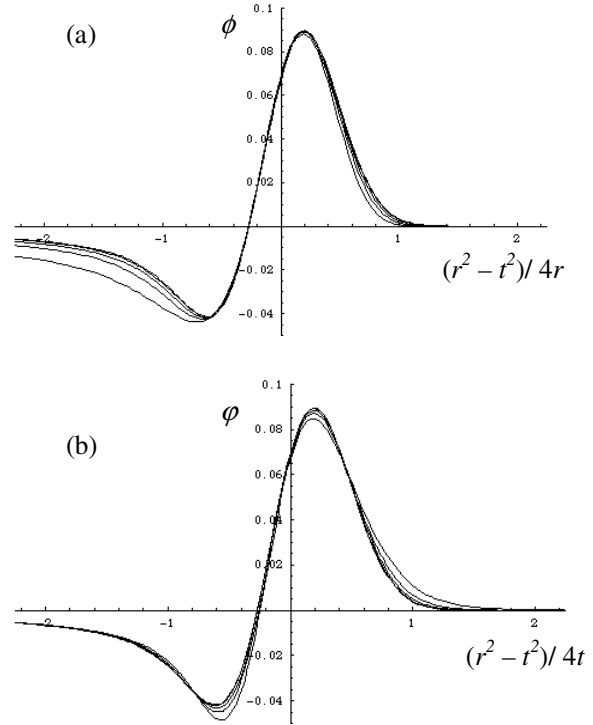


Figure 4 : Self-similar wave profile as t becomes large. Plotted are at $t = 5, 10, 20, 50,$ and 100 : a) $\phi([r^2 - t^2]/4r)$ in (11); b) $\phi([r^2 - t^2]/4t)$ in (12).

Inspired by the forms in (10), we attempt to plot the wave profiles in Fig. 4a as a function of r for each of $t = 5, 10, 20, 50,$ and 100 with the ordinate of:

$$\phi([r^2 - t^2]/4r) = \sqrt{r/50} \eta(r,t). \tag{11}$$

Figure 4a shows that the solution becomes self-similar when $t > 20$, approximately. Also note that for large t , it is anticipated that $t \sim r$ near the leading front, hence it is more convenient to plot the solution $\eta(r,t)$ with the slightly different ordinate

$$\phi([r^2 - t^2]/4t) = \sqrt{t/50} \eta(r,t), \tag{12}$$

and again the solution becomes self-similar when $t > 20$, as demonstrated in Fig. 4b. Henceforth we will use $\sqrt{50/t} \phi([r^2 - t^2]/4t)$ as though it were the exact description of the fundamental solution, η , for $t > 20$.

To provide an analytic recipe, we further made a curve fit to $\sqrt{50/t} \phi([r^2 - t^2]/4t)$ by trial-and-error inspection;

that is

$$\begin{aligned} \phi(s) &\approx M(s) \\ &= -0.0238 \frac{d}{ds} \begin{cases} (2s^2)^{1/4} K_{1/4}(2s^2) e^{-2s^2} & \text{for } s > 0, \\ (2s^2)^{1/4} \left\{ \begin{array}{l} K_{1/4}(2s^2) \\ + \pi\sqrt{2} I_{1/4}(2s^2) \end{array} \right\} e^{-2s^2} & \text{for } s < 0 \end{cases} \end{aligned} \tag{13}$$

where $s = [r^2 - t^2]/4t$, $I_{1/4}$ is the modified Bessel function of order $1/4$, and $K_{1/4}$ is the second modified (or hyperbolic) Bessel function of order $1/4$. Figure 5 provides a comparison of $\phi(s)$ with $M(s)$, which is seen to be indistinguishable.

2.2 Radiation from a Strip

We now explore the wave field that is generated by the water-surface displacement with the length L from the

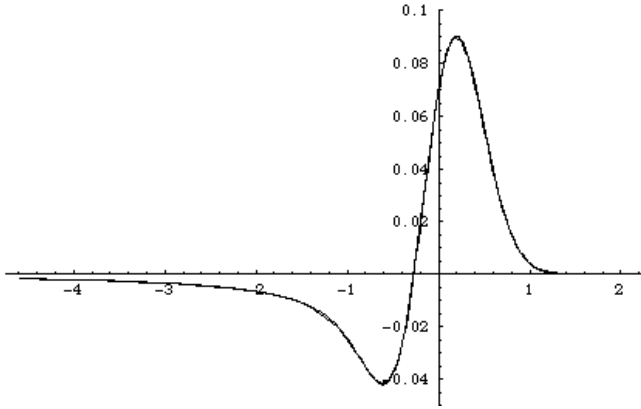


Figure 5 : Comparison of $\phi(s)$ and $M(s)$. $\phi(s)$ was plotted by setting $r = 50$. The both curves are indistinguishable.

position $x = X$ (see Fig. 1), which can be expressed as:

$$\begin{aligned} \eta(x, y, 0) &= \frac{1}{\sqrt{\pi}} \int_X^{X+L} 2e^{-[(x-x')^2+y^2]} dx' \\ &= [\text{erf}(X+L-x) - \text{erf}(X-x)] e^{-y^2}, \end{aligned} \quad (14)$$

and $\eta_t(x, y, 0) = 0$.

For the special case in which $X + L \rightarrow \infty$ and $X \rightarrow -\infty$, $\eta(x, y, 0) = 2e^{-y^2}$ is the initial condition for the infinite aspect ratio (one-dimensional) against which we wish to compare the finite aspect ratio results. The solution for the infinite aspect ratio is

$$\eta_{1-D}(y, t) = e^{-(t-y)^2}. \quad (15)$$

With finite X and L , $\eta(x, y, 0)$ is an initial displacement that is nearly uniform in x on the strip except in a small ($\delta x = O(1)$) neighborhood of its ends.

When $t > 20$, the solution of (1) with these initial conditions is

$$\begin{aligned} \eta(x, y, t) &\cong \frac{1}{\sqrt{\pi}} \int_X^{X+L} (50/t)^{1/2} \varphi\left(\frac{y^2-t^2}{4t} + \frac{x^2-x'^2}{4t}\right) dx' \end{aligned} \quad (16)$$

In particular, at $x = 0$ and $y = Y$,

$$\eta(0, Y, t) = \frac{1}{\sqrt{\pi}} \int_X^{X+L} (50/t)^{1/2} \varphi\left(\frac{Y^2-t^2}{4t} + \frac{x'^2}{4t}\right) dx'. \quad (17)$$

By changing the variable $x'^2/4t = \xi$, (17) becomes

$$\begin{aligned} \eta(0, Y, t) &= \sqrt{\frac{50}{\pi}} \int_{X^2/4t}^{(X+L)^2/4t} \varphi\left(\frac{Y^2-t^2}{4t} + \xi\right) \frac{d\xi}{\sqrt{\xi}} \\ &\cong \sqrt{\frac{50}{\pi}} \int_{(Y^2-t^2+X^2)/4t}^{(Y^2-t^2+(X+L)^2)/4t} \frac{M(s)}{\sqrt{s - (Y^2-t^2)/4t}} ds. \end{aligned} \quad (18)$$

It is an elementary numerical task to carry out this integration for any given combination of X , L , Y and t (see the definition sketch in Fig. 1). More appropriate notation for $\eta(0, Y, t)$ is

$$\eta(0, Y, t) = H(X, L, Y; t) \quad (19)$$

3 Results

We examine the following three initial displacements: $L = 10, 20$, and 40 as sketched in Fig. 6. The computed waveforms for $L = 20$ along three different directions ($\theta = 0, \pi/4$, and $\pi/2$) from the end of the source ($x = X$) are shown in Fig. 7. While the degradation of the wave height occurs immediately in the direction parallel to the major axis ($\theta = \pi/2$), the wave height does not change initially in the direction perpendicular to the major axis ($\theta = 0$). Note that the generated wave exhibits a two-signed waveform: the leading positive Gaussian-shaped wave followed by the negative wave. As the offset θ increases, the interval between the leading positive wave and the negative wave increases. In the case of $\theta = 0$, the leading positive wave and the subsequent negative wave are separated near the source. While those two are separated, the maximum amplitude remains constant at $\eta = 1/2$. We will discuss this pulse-persistence characteristic in details later. Also note that during the catching-up phase of the negative wave to the leading positive wave, the amplitude of the negative wave increases. On the other hand, both positive and negative amplitudes degrade for the case of $\theta = \pi/4$ and $\pi/2$.

Figure 8 shows the effects of the source elongation, $L = 10 - 60$. For the case of $L = 10$ and in the direction $\theta = 0$, the amplitude of the leading positive wave has already degraded at $r = 100$, although for the cases of $L > 20$, the maximum amplitude remains constant at 0.5 , as if the source is semi-infinitely long (X, ∞). This is because the negative wave generated at the other end of the strip has not reached the location $x = X$. In the direction of

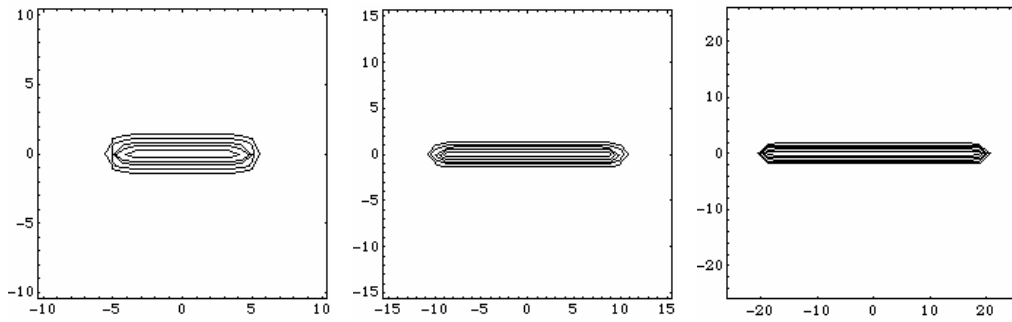


Figure 6 : Initial water-surface displacements of $L = 10, 20,$ and 40

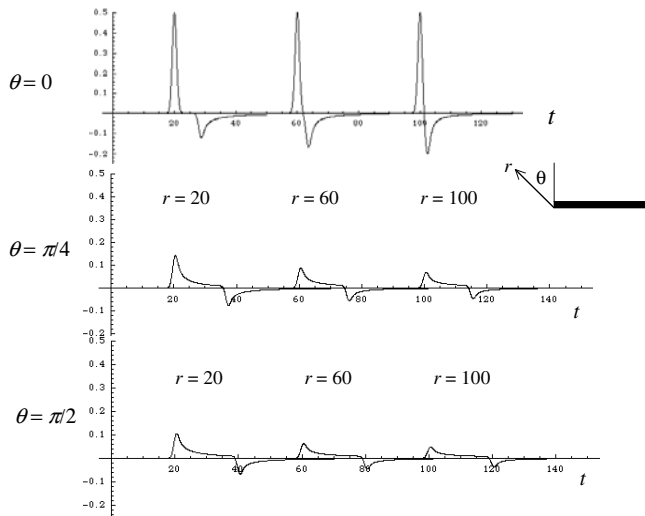


Figure 7 : Evolution of water-surface profiles $H(r; \theta; t)$ along the three different directions from the end of the source strip of the length $L = 20$

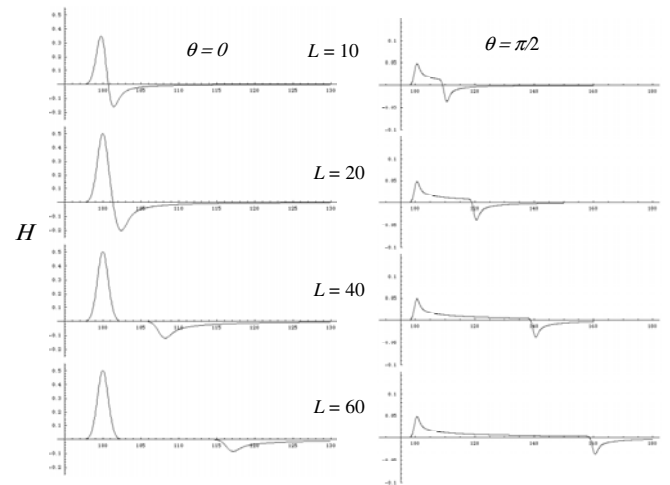


Figure 8 : The effects of the source elongation L on temporal water-surface variations at $r = 100$ in the directions normal ($\theta = 0$) and parallel ($\theta = \pi/2$) to the major axis from the end of the source strip ($X = 0$).

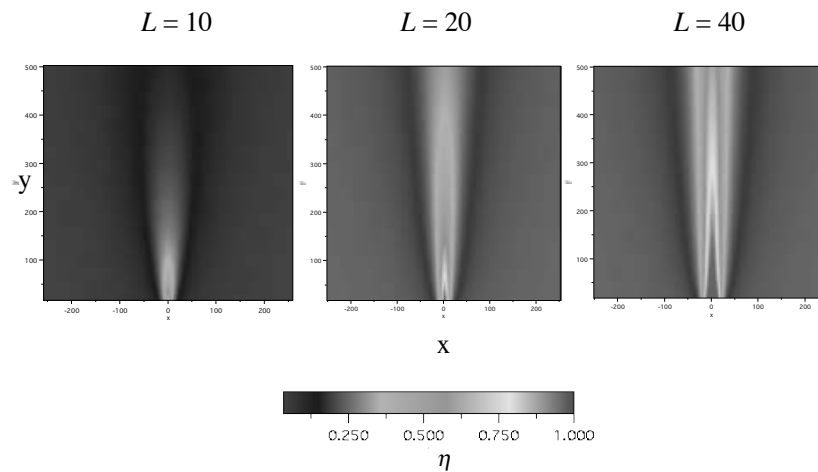


Figure 9 : The maximum water-surface elevations of the waves generated from the elongated source strip, $L = 10,$ $20,$ and 40

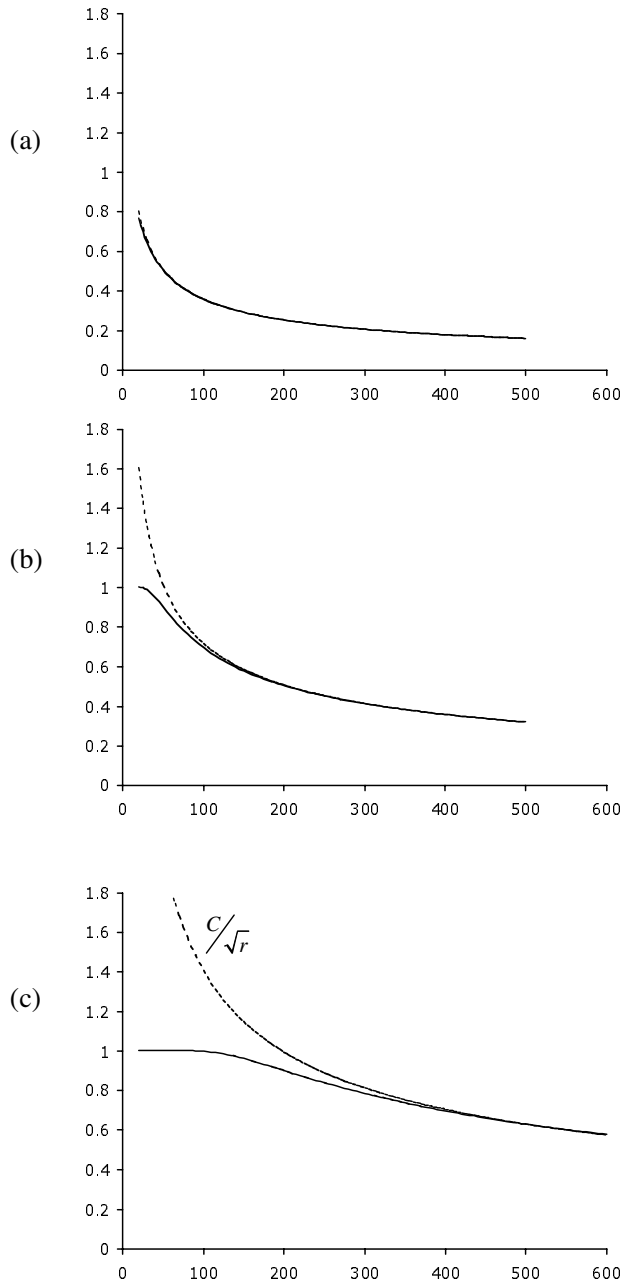


Figure 10 : Degradation of the maximum wave height along the bisector perpendicular to the source strip; a) $L = 10$, b) $L = 20$, c) $L = 40$. Note that the pulse persists until $Y_1 = 25$, and 100 in (b) and (c), as predicted in Fig. 11.

$\theta = \pi/2$, the separation between the positive and the negative wave remains constant at L . The amplitude of the leading wave is the same regardless the elongation L although the trailing negative wave is smaller for the larger

L owing to its longer propagation distance from the other end of the source. The mapping of the maximum water-surface elevations in the $x - y$ plane is shown in Fig. 9 for $L = 10, 20$, and 40 . Directivity of the elongated source is evident. Note that the origin of x is now placed at the mid point of the source. The degradation along y (perpendicular to the major axis of source elongation) at $x = 0$ (the center of the source) is plotted in Fig. 10 together with the fitted curve of C/\sqrt{r} . As expected, the degradation of the wave height with distance becomes $O(1/\sqrt{r})$ as r^2 becomes large enough. More dramatic, however, is the degradation of the wave height with increasing offset. The values of C are found to be 3.60, 7.18, and 14.09 for $L = 10, 20$, and 40 , respectively. The value of C appears to increase nearly linearly with L . Although not shown in Fig. 9, the degradation of the wave height along the x -axis at $y = 0$, i.e., along the major axis of the elongation, is found to be expressed with $C = 0.48$ regardless the value of L ; in this case, r is measured from the end of the source strip. Note that, for the case of the single Gaussian shaped blob expressed by (6), it is also found that $C = 0.48$

Observing Figs. 9 and 10, an interesting question is: for a given L and with $x = X$, what is the largest distance Y at which the strength of the arriving pulse from the finite source differs very little from the strength of the pulse emanating from the source line extending from X to $+\infty$? Equation (17) states that the integral that gives the value of η at any y and at time $t = Y$ is the integral of $\sqrt{50/t} \varphi([y^2 + x^2 - t^2]/4t)$ from $x = X$ to L . We also know that the same integrand, when integrated over $X < x < \infty$ gives $\eta = (1/2)\eta_{1-D}$ at $x = X$. However, for small y there is no significant contribution of that integrand to the latter integral and therefore one can be certain that the leading part of the wave from the source of length L differs negligibly from the wave produced by the source lying in (X, ∞) . In particular, let Y_1 be that y above which, at time t , the 1-D Gaussian from the ∞ source would be confined. Then, it follows from the foregoing that the full 1-D Gaussian distribution of η arrives at Y if $Y_1^2 + L^2 \geq (Y_1 + Q)^2$, where Q is the breadth of the Gaussian pulse. The schematic diagram in Fig. 11 shows that the full Gaussian pulse emanating from $x = L$ reaches the tail of the Gaussian wave at $t = Y_1 + Q$ at the location $Y = Y_1$. If we take $Q = 4$, that is 1.8 % of the wave height, which we consider negligible, then we find $Y_1 \leq L^2/8$.

One can repeat this argument when the question concerns

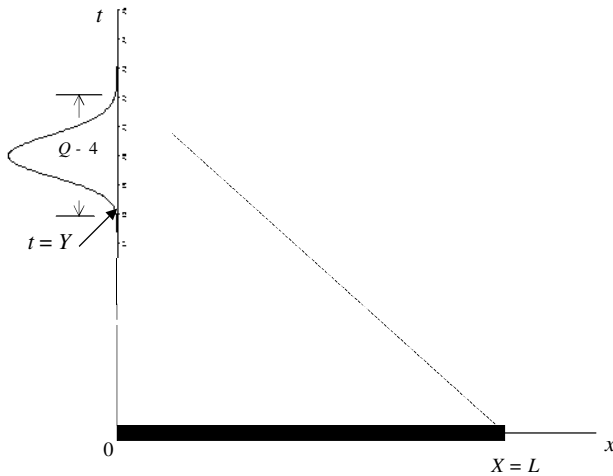


Figure 11 : A schematic diagram for the pulse persistence. The pulse emanating from $X = L$ does not reach at Y until $t = Y + Q$. The tail end of the Gaussian pulse indicated by Q is already so small (1.8% of the wave height if $Q = 4$) to be considered negligible

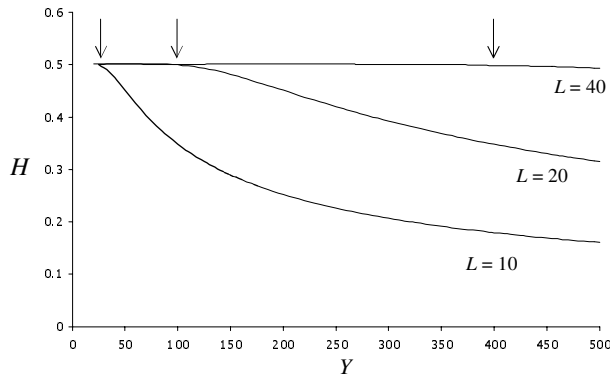


Figure 12 : Degradation of the maximum wave height in the direction perpendicular to and from the end of the major axis of the source strip. The locations of pulse-persistent limit Y_1 , shown by the arrow, are $Y_1 = 25, 100,$ and 400 for $L = 10, 20,$ and 40 , respectively

the arrival of the maximum wave height rather than the full Gaussian. In that case a smaller value $Q/2$ is pertinent, i.e. $Y_1 \leq L_1^2/4$. As for the direction of the perpendicular bisector of the source ($x = X + L/2$), it is trivial to show that the pulse persists for the order of $Y_1 \leq L_1^2/16$ without significant diminution from the infinite-strip intensity. In dimensional term, that distance is $\ell^2/16\beta$. The locations of Y_1 for $L = 10, 20,$ and 40 are $6.26, 25,$ and

100 , respectively: Y_1 for $L = 10$ is too short to be detected in Fig.10. In the direction perpendicular to the major axis from the end of source ($x = X$), the locations of Y_1 are shown in Fig. 12 together with the variations of the maximum wave-height profiles.

4 Conclusions

Based on classical linear shallow-water-wave theory, a convenient methodology is developed to compute the wave propagation across a region of finite depth from an elongated tsunami source with large but finite aspect ratio. A similar problem was previously solved by Kajiura (1970) for uniform and linear source displacements, but the complexity of his integrals disallowed detailed analyses for quantitative physical interpretation, in particular for large t . Apart from Kajiura (1970), we utilize the solution algorithm for general initial-valued problem of 2-D axisymmetric waves. Using that algorithm with the initial displacement of Gaussian shape, a convenient form of the self-similar solution is derived, which yields a very accurate representation except in the region very close to the source. Using this solution as a Green's function, tsunami propagation from an elongated source is solved by integration.

Interesting, but not surprising in view of the structure of the solution ϕ , is the development of a two signed waveform. The degradation in wave height enhances with increasing offset of the propagation direction from the line perpendicular to the major axis of source elongation. This is a well-known characteristic of the directivity. The asymptotic behavior of the degradation rate is $O(1/\sqrt{r})$ as expected. Near the source, however, the pulse persists without significant diminution from the infinitely long source intensity. Along the propagation perpendicular to the major axis, the pulse-persistent distances were found to be $L_1^2/16$ and $L_1^2/4$ from the mid point and the end of the source strip, respectively. Note that the wave height in the pulse-persistent region from the mid point is twice the wave height emanating from the end of the source strip. For a large distance where the wave height decays proportional to $1/\sqrt{r}$, the propagation from the mid point of the source strip behaves as if the source is the axisymmetric Gaussian with the enhanced amplitude by $0.74L$. On the other hand, the wave height decreases immediately in the direction parallel to the major axis regardless of the length of the source strip, L ; in fact the degradation is the same as that from the equivalent axisymmetric

Gaussian source.

The sea-floor displacement that caused the December 26, 2004 Sumatran tsunami was roughly 800 km long and 150 km wide (e.g. Ammon, et al., 2005). If 90% of the volumetric displacement is confined within the 150 km breadth, then it is reasonable to take the characteristic source breadth scale $\beta = 45$ km for the Gaussian shaped source represented by (14). This tsunami surface profile was measured by the Jason-1 laser altimetry satellite (e.g. Hirata et al., 2005; Gower, 2005). The altimetry data show that the maximum elevation of the leading wave was approximately 0.75 m at the location (Latitude 4° S, Longitude 84° E). This location is about 1600 km away from the epicenter, and in the direction normal to the ruptured fault, crossing the southern end. This circumstance is equivalent to $L \approx 17.8$, $Y \approx 35.5$, $X \approx 0$, and $\theta = 0$ (see Fig. 1). Based on our analysis, the pulse persists until $Y < L^2/4$, or 3,600 km from the source, which is well beyond the location of the measurement (1,600 km). Since the persistent pulse from the end of the source ($X = 0$) has one-half the amplitude of that at the mid point, and the initial static displacement of the surface is twice the amplitude of the persistent pulse emanating from the mid point, we can infer that the initial vertical displacement by the earthquake is approximately 3 m, which is in good agreement with the estimate made with the seismic signals by Ammon, et al. (2005). It must be cautioned that our forgoing computation assumes that an equal amount of wave energy be propagated in the opposite direction, i.e., toward Thailand and Myanmar. Regardless, our model provides a simple tool for a quantitative estimation of tsunami propagation from a finite source.

5 Remarks

The basic mathematics described in this paper was presented by the late Professor George Carrier in 1990 at the 2nd UJNR Tsunami Workshop, Honolulu. The workshop was supported by a National Science Foundation grant through Dr. Cliff Astill's program. Dr. Astill attended the workshop and since then, he encouraged Carrier working on tsunami by supporting his research and including him in a collaborative tsunami research team. Dr. Astill's vision and support made fundamental advances in tsunami research. In this paper, Carrier's original work presented at the workshop was corrected, revised, and improved by adding interpretations, figures,

and examples.

Acknowledgement: GC acknowledged the collaboration of B. Budiansky and J.W. Hutchinson. The work was supported by the US National Science Foundation (CMS-0245206).

References

- Ammon, C.J.; Ji, C.; Thio, H.-K.; Robinson, D.; Ni, S.; Hjorleifsdottir, V.; Kanamori, H.; Lay, T.; Das, S.; Helmberger, D.; Ichinose, G.; Polet, J.; Wald, D.** (2005): Rupture process of the 2004 Sumatra-Andaman Earthquake, *Science*, vol. 308, pp. 1133-1139
- Ben-Menahem, A.** (1961): Radiation of seismic-surface-waves from finite moving source, *Bull. Seism. Soc. Am.*, vol. 51, pp. 401-435.
- Carrier, G.F.** (1966): Gravity waves on water of variable depth. *Journal of Fluid Mechanics*, vol. 24, p. 641-659
- Carrier, G.F.** (1971): Dynamics of tsunamis. In: W.H. Reid (ed) *Mathematical Problems in the Geophysical Sciences. -Vol. 1 Geophysical Fluid dynamic*, American Mathematical Society.
- Carrier, G.F.; Wu, T.T.; Yeh, H.** (2003): Tsunami Runup and Drawdown on a Plane Beach, *Journal of Fluid Mechanics*, vol. 475, pp. 79-99
- Gower, J.** (2005): Jason 1 detects the 26 December 2004 Tsunami, *EOS, Trans. Amer. Geophys. Union*, vol. 86, pp. 37-38.
- Hammack, J.L.; Segur, H.** (1978): Modelling criteria for long water waves. *J. Fluid Mech.*, vol. 84, 359-373.
- Hirata, K.; Satake, K.; Tanioka, Y.; Kuragano, T.; Hasegawa, Y.; Hayashi, Y.; Hamada, N.** (2005): The 2004 Giant Sumatra Earthquake source model from satellite altimetry. presented at the AOGS 2nd Annual Meeting in Singapore, June 20-24, 2005.
- Kajiura, K.** (1970): Tsunami source, energy and the directivity of wave radiation. *Bulletin Earthquake Research Institute*, vol. 48, pp. 835-869.
- Okal, E.A.** (2003): Normal mode energetics for far-field tsunami generated by dislocations and landslides, *Pure Appl., Geophys.*, vol. 160, pp. 2189-2221.
- Takahashi, R.; Hatori, T.** (1962): A model experiment on the tsunami generation from a bottom deformation area of elliptic shape. *Bulletin Earthquake Research Institute*, vol. 40, pp. 873-883. (in Japanese).

